SCIENTIFIC REPORTS

OPEN

SUBJECT AREAS:
RENEWABLE ENERGY
ELECTROCATALYSIS
HETEROGENEOUS CATALYSIS
NANOPARTICLES

Received
1 July 2014

Accepted
10 October 2014

Published
30 October 2014

Correspondence and requests for materials should be addressed to X.Q. (quanxie@dlut.edu.cn)

Efficient and durable hydrogen evolution electrocatalyst based on nonmetallic nitrogen doped hexagonal carbon

Yanming Liu, Hongtao Yu, Xie Quan, Shuo Chen, Huimin Zhao & Yaobin Zhang

Faculty of Chemical, Environmental and Biological Science and Technology, Dalian University of Technology, Dalian 116024, China.

The feasibility of renewable energy technology, hydrogen production by water electrolysis, depends on the design of efficient and durable electrocatalyst composed of earth-abundant elements. Herein, a highly active and stable nonmetallic electrocatalyst, nitrogen doped hexagonal carbon (NHC), was developed for hydrogen production. It exhibited high activity for hydrogen evolution with a low overpotential of only 65 mV, an apparent exchange current density of 5.7×10^{-2} mA cm^{-2} and a high hydrogen production rate of 20.8 mL cm^{-2} h^{-1} at −0.35 V. The superior hydrogen evolution activity of NHC stemmed from the intrinsic electrocatalytic property of hexagonal nanodiamond, the rapid charge transfer and abundance of electrocatalytic sites after nitrogen doping. Moreover, NHC was stable in a corrosive acidic solution during electrolysis under high current density.

Hydrogen evolution reaction (HER) is critical for a variety of important areas such as water electrolysis, chlor-alkali electrolysis, metal deposition and corrosion protection[1]. In particular, sustainable and efficient hydrogen production from water electrolysis has attracted growing scientific interest because hydrogen, a clean and renewable energy carrier, is a promising alternative for traditional fossil fuels in the future[2]. The efficiency of electrocatalytic hydrogen production strongly depends on the electrocatalyst. An advanced electrocatalyst for HER should reduce the overpotential and consequently increase hydrogen production efficiency[3]. Pioneering studies have demonstrated Pt-group metals exhibit low overpotential and fast kinetics for HER, which are the most effective electrocatalysts[4]. However, the high cost and rarity of these noble metals make their large-scale applications unattractive.

Recently, both organometallic complexes and inorganic electrocatalysts based on transition metals have been proposed to be potential substitutes of Pt-group metals[5–9]. However, for organometallic complexes, further study needs to address issues related to low activity in aqueous solution as well as the limited stability due to their inherent susceptibility to decomposition[10]. On the other hand, fully inorganic electrocatalysts such as transition metal chalcogenides, carbides, and nitrides are highly appealing[11–13]. As a result, many attempts have been made to improve their HER activity through increasing electrocatalytic sites and conductivity by introducing Au and graphitic carbon[14–18]. Meanwhile, intense research efforts have been made on nonmetallic electrocatalysts, resulting in the development of polyhydroxylated fullerene and carbon nitride for hydrogen evolution[19,20]. Despite tremendous efforts, many researches still focus on developing highly active and durable HER electrocatalysts based on earth abundant, nonmetallic components.

Doped cubic diamond is a favorable electrocatalytic material in many fields owning to its high electrocatalytic activity, extended lifetime, good mechanical and chemical stability[21]. Unfortunately, its high overpotential for HER makes it unattractive for water electrolysis[22], but hexagonal nanodiamond, combining the cubic structure of cubic diamond and the layered hexagonal structure of graphite[23], may possess the outstanding properties of cubic diamond while offering a high conductivity and low overpotential for HER. The HER performance of hexagonal nanodiamond probably can be enhanced by synergistic coupling with graphite, which has been reported as HER catalyst support due to its abundance of electrochemically active edges, large surface area, high conductivity and low cost[24,25]. Furthermore, the electrocatalytic activity of carbon materials can be further improved by heteroatom doping[26]. When nitrogen atoms are doped into a carbon framework, it can increase the catalytic sites through inducing strain and defect sites[27]. Nitrogen doping also can polarize adjacent carbon atoms, and thereby may induce a reduced energy barrier towards electrochemical reactions[28]. Hence N-doped hexagonal carbon (NHC), composed of hexagonal nanodiamond and graphite, was first designed as a novel HER electrocatalyst in this work.

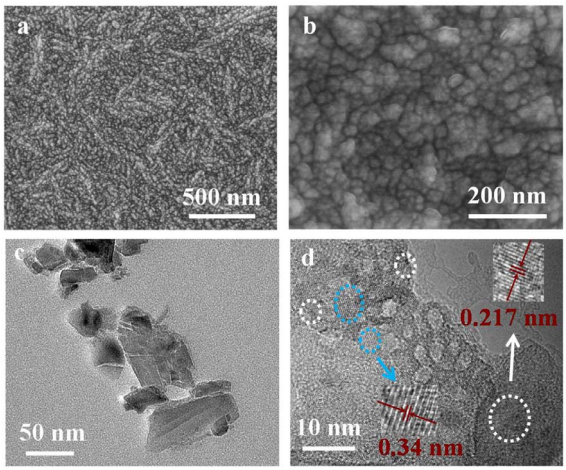

Figure 1 | SEM and TEM images of NHC electrode. (a,b)SEM images and (c,d) TEM images of NHC electrode.

In an effort to develop economical material for replacing noble metal as HER electrocatalyst, we reported an efficient, stable and metal-free HER electrocatalyst based on NHC. Its HER performance was evaluated by testing its polarization curve, hydrogen production rate and long-time durability, whereas the HER mechanism was analyzed by Tafel slope. Meanwhile, the HER behaviors of commercial Pt/C, hexagonal carbon (HC) and graphite were also examined as comparison. For NHC, the origin of its activity was discussed.

Results

NHC electrode was prepared by depositing NHC film on Ti substrate using microwave plasma enhanced chemical vapor deposition. Figure 1a displays the scanning electron microscopy (SEM) image of prepared NHC electrode, which reveals a uniform NHC film with characteristic 'ridge' like structure is deposited on Ti substrate. This NHC film appears to cover the entire substrate without any noticeable cracks. The high resolution SEM image (Figure 1b) shows the 'ridge' is composed of nanoparticles. The size of these nanoparticles is in the range of 10 ~ 80 nm, as estimated from the transmission electron microscopy (TEM) image of Figure 1c and 1d. The measured interplanar spacing are 0.217 nm and 0.34 nm, corresponding to the (100) plane of hexagonal diamond and (002) plane of graphite, respectively.

The X-ray diffraction (XRD) pattern of NHC electrode is presented in Figure 2a. Diffraction peaks appear at 41.3°, 43.9°, 75.4°, 82.4° and 91.6° are corresponding to (100), (002), (110), (013) and (112) facets of hexagonal diamond, respectively (JCPDS no.19-0268). The peaks observed at 36.1°, 60.7° and 72.7° are related to the formation of TiC layer between Ti substrate and NHC film. TiC layer can be formed when diamond was grown on the Ti substrate by chemical vapor deposition[29]. Three peaks can be observed in the Raman spectroscopy (Figure 2b). The peak located at 1170 cm^{-1} is attributed to the E_{2g} mode of hexagonal nanodiamond. A broad asymmetrical peak appears at 1250 cm^{-1} ~ 1425 cm^{-1}, which can be deconvoluted into two peaks (1321 cm^{-1} and 1360 cm^{-1}) by Gaussian fitting. The peak at 1321 cm^{-1} is the A_{1g} mode of hexagonal nanodiamond. The other peaks around 1360 cm^{-1} and 1540 cm^{-1} arise from graphite. X-ray photoelectron spectroscopy (XPS) N 1s spectrum (Figure 2c) demonstrates nitrogen atoms have been successfully doped into NHC. The peak at 398.8 eV corresponds to N atoms bonded with sp^3-hybridized C atoms (N-sp^3C), while the peak at 400.0 eV corresponds to N atoms bonded with sp^2-hybridized C atoms (N-sp^2C)[30,31]. The N-N bonds may be related to encapsulated nitrogen[30]. These results reveal that incorporated nitrogen mainly exists as N-sp^2C and N-sp^3C bonds. The amount of doped nitrogen is 1.1 at.% from XPS element analysis. In order to identify the content of hexagonal nanodiamond and graphite in NHC electrode, XPS C 1s spectrum (Figure 2d) is deconvoluted into four peaks, related to sp^3 C-C bond, sp^2 C-C bond, sp^3 C-N bond and sp^2 C-N bond, respectively[31]. According to their peak areas, the ratio of (sp^3 C-C + sp^3 C-N)/(sp^2 C-C + sp^2 C-N) is about 1.35, which is approximately equal to the ratio of hexagonal nanodiamond to graphite.

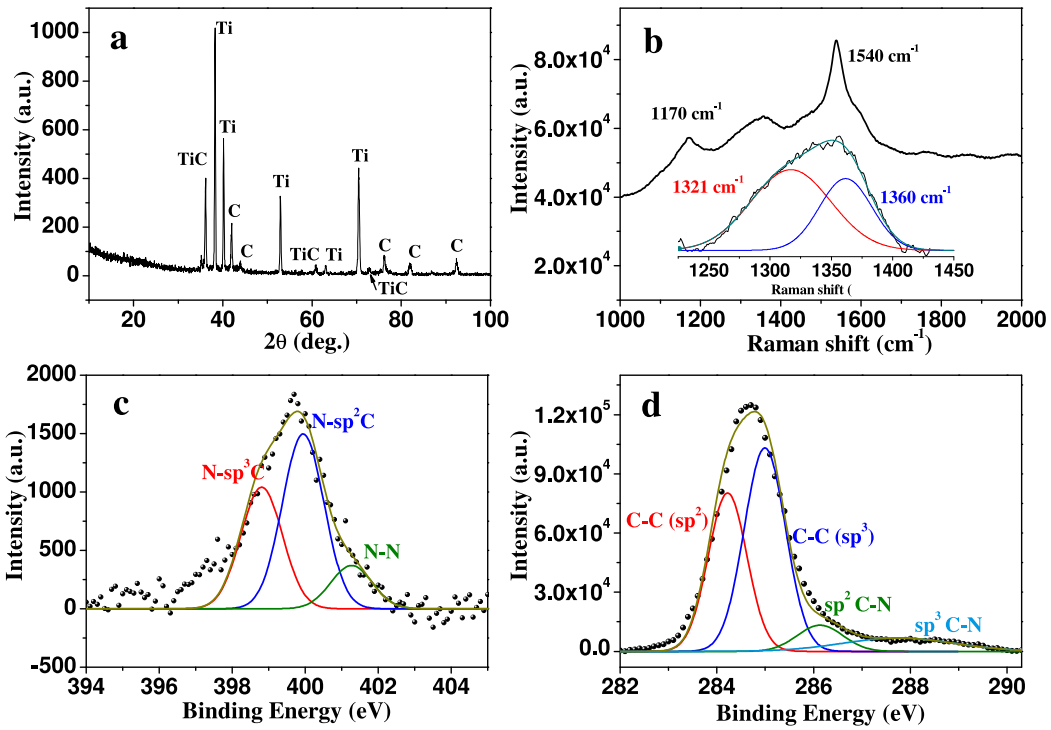

Figure 2 | XRD, Raman and XPS spectra of NHC electrode. (a) XRD spectrum. (b) Raman spectrum. (c) XPS N 1s spectrum. (d) XPS C 1s spectrum.

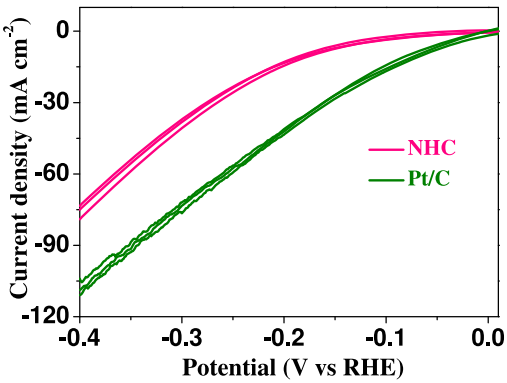

Figure 3 | HER activity of different electrodes. Linear sweep voltammograms of commercial Pt/C and NHC electrodes in 0.5 M H_2SO_4 (scan rate 5 mV s^{-1}).

The electrocatalytic activity of NHC electrode for hydrogen evolution was investigated by linear sweep voltammetry in 0.5 M H_2SO_4 solution. As a comparison, the HER activity of commercial Pt/C electrode was also tested. As presented in Figure 3, the polarization curve of NHC electrode shows a small onset potential of −65 mV for HER, beyond which the cathodic current density increases rapidly under more negative potentials. This is one of the most positive onset potentials for electrocatalytic HER among the reported non-noble materials[18,20,32] (Details in Supplementary Table S1), which is comparable to that of commercial Pt/C electrode (0 V). This result suggests NHC electrode may favor proton reduction kinetics. For driving a current density of 10 mA cm^{-2}, NHC electrode only requires an overpotential of 0.18 V, which is comparable or even lower than those of reported nonprecious electrocatalysts[17,18,20,32]. These results imply that fast and efficient electron transfer occurs on the NHC electrode. In addition, NHC electrode is also active for HER at neutral and basic solution (Supplementary Fig. S1).

Figure 4 shows the hydrogen amount produced on NHC electrode under Galvanostatic electrolysis in 0.5 M H_2SO_4. The hydrogen production rate is normalized by electrode area. NHC presents high hydrogen production rates at low overpotentials, which are 3.24 mL cm^{-2} h^{-1} and 20.8 mL cm^{-2} h^{-1} at electrolysis potential of −0.15 V and −0.35 V, respectively. Under potentials both −0.15 V and −0.35 V, the amount of hydrogen experimentally quantified by gas chromatography during electrolysis matches well with the values calculated theoretically from the number of charges passing through the electrode, indicating high hydrogen production efficiency (nearly 100%) of NHC electrode. These results clearly confirm the high electrocatalytic activity of NHC electrode.

A promising material for electrocatalytic HER should exhibit not only high activity but also good durability. The long-term stability of NHC electrode was examined by electrolysis at high current density in 0.5 M H_2SO_4. As shown in Figure 5a, although NHC electrode is operated in a corrosive acidic solution at overpotential 0.27 V, its cathodic current density remains around 30.4 mA cm^{-2} for 30 h operation. After 10,000 cycles of potential sweeps at -0.4 ~ 0.6 V, NHC electrode retains a polarization curve similar to the initial one with negligible loss of cathodic current density (Figure 5b). These results demonstrate that NHC electrode is durable during electrocatalytic hydrogen production. Its stability compares well with those of other newly reported noble-metal free electrocatalysts[19,32,33], while NHC electrode is still in the series displaying the best performance so far. The excellent durability of NHC electrode arises from the superior electrochemical stability and corrosion resistance of nanodiamond.

Discussion

In order to clarify the factors contributed to the good HER performance of NHC electrode, the HER activity of HC electrode was measured as the reference (Figure 6). The onset potential for HER at NHC electrode is more positive than that at HC electrode, and the current density of NHC electrode is also larger than that of HC electrode when the potential is more negative than −0.07 V, indicating the HER activity of NHC electrode is obviously enhanced after nitrogen doping. When nitrogen amount increases from 0 to 1.1 at.%, current density of NHC electrode at the same potential is significantly enhanced (Supplementary Fig. S2). However, the enhancement is not obvious when the nitrogen amount is further increased to 1.5 at.%. Therefore, NHC electrode with nitrogen content 1.1 at.% is selected for the following experiments. Since graphitic carbon (sp^2-C) exists in NHC electrode, HER activity of graphite, N-doped graphite and NHC with different contents of sp^2-C were also tested to evaluate its contribution (Supplementary Fig. S3). Cathodic current from hydrogen evolution is observed on graphite and N-doped graphite electrodes, indicating the sp^2-C in NHC electrode may contribute to HER activity. To further clarify the contribution of sp^2-C, NHC electrodes with different sp^2-C contents were prepared (Supplementary Table S2). The HER activity of NHC electrode is enhanced when the sp^2-C content increases from 32.9% (sp^2/sp^3 = 0.49, NHC1) to 42.5% (sp^2/sp^3 = 0.74, NHC2) and almost keep constant by further increasing the sp^2-C content to 50.5% (sp^2/sp^3 = 1.02, NHC3). This phenomenon is correlated to their charge transfer resistance (NHC1 > NHC2 ≈ NHC3, Supplementary Fig. S4). The increased sp^2-C content in NHC electrode facilitates charge transfer to some extent and thereby results in improved HER activity. Compared with N-doped graphite, NHC electrode presents significantly enhanced HER activity with much lower overpotential and

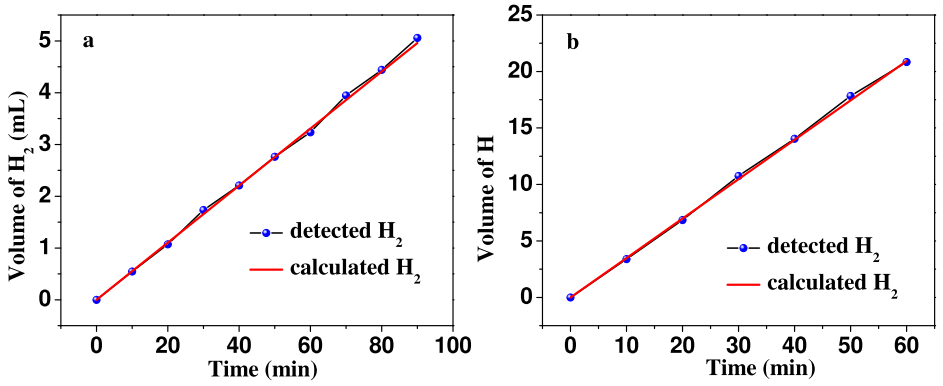

Figure 4 | Hydrogen produced practically and theoretically. The volume of hydrogen calculated and detected on NHC electrode in 0.5 M H_2SO_4 at potential (a) −0.15 V (vs RHE) and (b) −0.35 V (vs RHE).

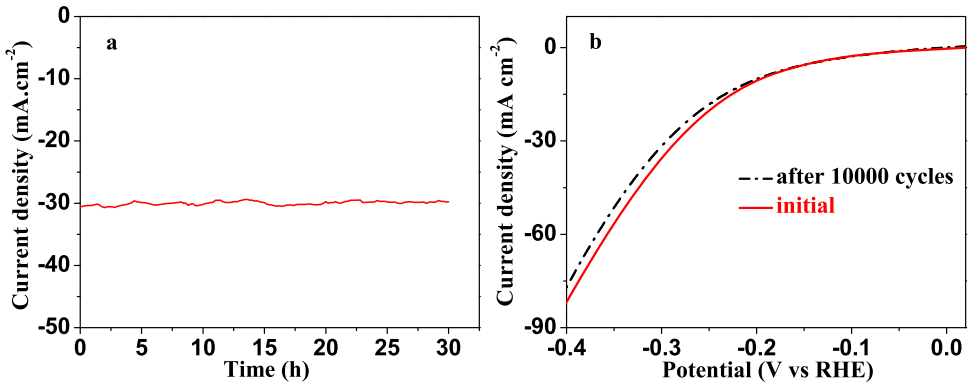

Figure 5 | Stability of NHC electrode for HER. (a) Time dependence of electrocatalytic current density during electrolysis at overpotential 0.27 V for NHC electrode. (b) Polarization curves of NHC electrode before and after potential sweeps (-0.4 ~ 0.6 V, 100 mV s^{-1}) for 10,000 cycles in 0.5 M H_2SO_4.

larger current density, suggesting the HER activity of NHC electrode is mainly originated from hexagonal nanodiamond and/or the synergistic effect between hexagonal nanodiamond and graphitic carbon. These results indicate that graphitic carbon in NHC can facilitate hydrogen evolution to some extent, but it is not the main factor contributed to the high HER activity of NHC. Since it is difficult to separate TiC from NHC film, commercial TiC is employed for comparison. It should be noticed that the Ti electrode shows a very negative onset potential for HER with almost neglectable current density in the potential range of −0.4 V ~ 0 V, while both commercial TiC (99.99%, cubic, 20 nm) and commercial TiN (99.9%, cubic, 20 nm) exhibit more negative onset potential and much lower current density than NHC electrode (Supplementary Fig. S5). Moreover, Auger depth profile shows Ti content at the surface layer (thickness about 2 μm) of NHC electrode is lower than the detection limit (Supplementary Fig. S6), which indicates the HER activity of NHC electrode is originated from NHC film. Inductively coupled plasma atomic emission spectroscopy (ICP-AES) was performed to rule out metal contamination (Supplementary Table S3) of NHC film. The results suggest the HER activity of NHC electrode is originated from NHC film rather than metal impurities. CO adsorption has further confirmed the absence of Pt at NHC electrode (Supplementary Fig. S7). These results demonstrate HER activity of NHC electrode is mainly originated from hexagonal nanodiamond and/or the synergistic effect between hexagonal nanodiamond and graphite as well as nitrogen doping.

To obtain further insight into the good activity of NHC electrode for electrocatalytic HER, electrochemical impedance spectroscopy analysis was used to characterize its charge-transfer rate for HER. The Bode plots reveal single time constant behavior of these electrodes (Supplementary Fig. S8). Based on the Bode and Nyquist plots (Figure 7), corresponding equivalent circuit model is obtained (Supplementary Fig. S8). The charge-transfer resistance is determined from the diameter of semicircle at high frequencies in Nyquist plot. The NHC electrode presents a charge-transfer resistance of 59.3 Ω, much smaller than that of HC electrode (116.1 Ω). It reveals the charge-transfer resistance of NHC electrode is significantly decreased after nitrogen doping, which will result in a much faster electron transfer from active sites of NHC to protons during HER. The charge-transfer resistance of graphite electrode is 59.9 Ω, comparable to that of NHC electrode, but the HER performance of NHC electrode is advantageous over that of graphite electrode. In addition, the electrical resistivity is 2.07 mΩ cm for NHC and 1.69 mΩ cm for graphite, much smaller than that of HC (12369.8 mΩ cm), indicating the good conductivity of NHC and graphite. These results illustrates the enhanced electrocatalytic activity of NHC electrode for HER can be attributed to the high rate of electron transfer after nitrogen doping and the intrinsic electrocatalytic property of HC.

Tafel slope is an inherent property of electrocatalytic material. It is determined by the rate-limiting step of HER. The determination and interpretation of Tafel slope are important for elucidation of the hydrogen evolution mechanism involved. The linear portions of Tafel plots on NHC (50 ~ 89 mV), HC (87 ~ 208 mV) and commercial Pt/C electrodes (4 ~ 29 mV) were fitted to the Tafel equation, as displayed in Figure 8. The determined Tafel slopes are 56.7, 109.5, 30.3 mV dec^{-1} for NHC, HC and commercial Pt/C electrodes, respectively. The Tafel slope of NHC electrode is not only smaller than that of HC electrode, but also smaller than those of many non-noble electrocatalytic materials reported recently, such as Cu_2MoS_4 (95 mV dec^{-1})[18], $C_{60}(OH)_8$ (78 mV dec^{-1})[20], Mo_2S/Au (69 mV dec^{-1})[17] and Mo_2C/XC (59.4 mV dec^{-1})[16] (Details in Supple-

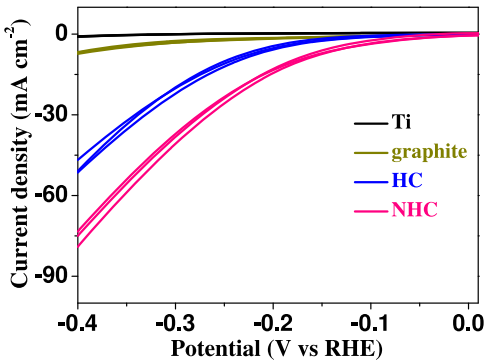

Figure 6 | HER activity of different electrodes. Linear sweep voltammograms of NHC, HC, graphite and Ti electrodes in 0.5 M H_2SO_4 (scan rate 5 mV s^{-1}).

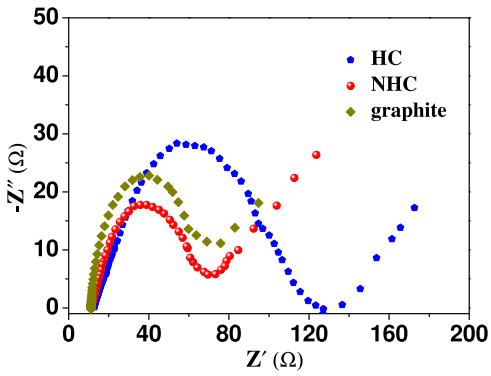

Figure 7 | Comparison of charge-transfer resistances. Nyquist plots of graphite, HC and NHC electrodes in 0.5 M H_2SO_4 solution.

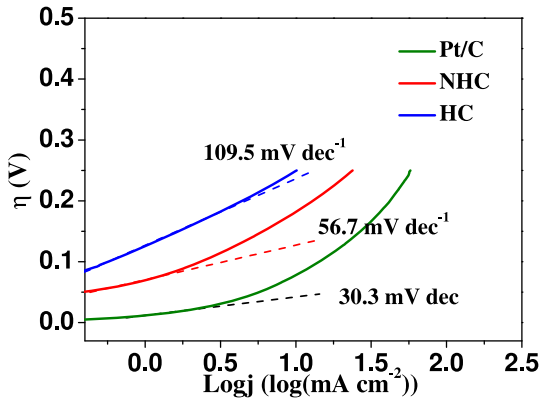

Figure 8 | Tafel plots of different electrodes. Tafel plots of NHC, HC and Pt/C electrodes in 0.5 M H_2SO_4 (scan rate 5 mv s^{-1}).

mentary Table S1). The smaller Tafel slope of NHC electrode will lead to a faster increment of reaction rate with increasing overpotential. The exchange current density is obtained from Tafel curve by using extrapolation method, which is 5.7×10^{-2} mA cm^{-2} for NHC electrode. This value is higher than those found for the above mentioned nonprecious electrocatalytic materials ($7.0 \times 10^{-5} \sim 4.0 \times 10^{-2}$ mA cm^{-2}). Compared with those non-noble electrocatalytic materials reported recently, NHC electrode presents a quite large exchange current density and a relatively small Tafel slope at such low overpotential, indicating NHC is a promising nonmetallic electrocatalyst for HER. According to the two-electron-reaction model, electrocatalytic HER at acidic media proceeds in two steps. First is the discharge step (Volmer reaction, $2H_3O^+ + M + e^- \rightarrow M\text{-}H + H_2O$, 116 mV dec^{-1}). Second is the electrochemical desorption step (Heyrovsky reaction, $H_3O^+ + M\text{-}H + e^- \rightarrow M + H_2 + H_2O$, 40 mV dec^{-1}) or the recombination step (Tafel reaction, $M\text{-}H + M\text{-}H \rightarrow M + H_2$, 30 mV dec^{-1}). The obtained Tafel slope of 56.7 mV dec^{-1} suggests that hydrogen evolution on NHC electrode probably occurs via a Volmer–Heyrovsky mechanism. The relatively small slope indicates fast proton discharge kinetics on NHC electrode.

Based on the aforementioned results, the superior HER activity of NHC electrode is considered to stem from the inherent hydrogen evolution property of HC as well as the improved charge transfer kinetics and increased catalytic sites after nitrogen doping. The excellent HER performance of HC is benefited from the unique structure of hexagonal nanodiamond and/or the synergistic effect between hexagonal nanodiamond and graphite. It has been proved the HER activity is further improved by nitrogen doping, which can significantly improve the charge transfer kinetics. Nitrogen doping also can polarize adjacent carbon atoms and the positively charged carbon atoms can act as active sites for hydrogen adsorption (Supplementary Fig. S9). It may facilitate the Volmer reaction and thereby can induce a reduced energy barrier towards HER[34]. Besides, defects induced by nitrogen doping can acts as active sites for electrochemical reduction reaction[28].

In summary, an efficient and durable hydrogen evolution electrocatalyst, NHC, has been created from earth abundant and nonmetallic components. NHC electrode exhibited superior performance for HER with a low overpotential (65 mV) and a large exchange current density (5.7×10^{-2} mA cm^{-2}). Moreover, NHC electrode showed high hydrogen production rate (20.8 mL cm^{-2} h^{-1} at overpotential of 0.35 V) and good stability during electrolysis. These outstanding behaviors of NHC were attributed to the excellent electrocatalytic HER activity of HC, remarkably reduced charge-transfer resistance and increased catalytic sites after N doping. This work indicates NHC represents a new and attractive nonmetallic inorganic material for water electrolysis, which is valuable in exploring related nonmetallic or all-carbon based electrocatalyst for HER.

Methods

Preparation of Electrodes. The NHC electrode was prepared by microwave plasma enhanced chemical vapor deposition (MMPS-2030C, Chengdu Hueray microwave Tech. Ltd) under the following conditions: a gas mixture of $H_2/CH_4/N_2$ (CH_4 = 10 ~ 20%, N_2 = 0.4~1.2%), substrate temperature of 480°C, pressure of 6.0 ~ 6.1 kPa and deposition time of 4 h. As a comparison, HC electrode was synthesized under the same conditions for NHC electrode preparation but without adding N_2. The commercial Pt/C electrode was prepared as follows: commercial Pt/C catalyst (20 wt% Pt on Vulcan carbon black) was dispersed in Nafion/ethanol solution by at least 30 min sonication to form a homogeneous ink, and then the catalyst ink was drop-coated onto Ti substrate (6 mm in diameter) with a catalyst loading of 0.35 mg cm^{-2}.

Characterization. SEM images were recorded on a Hitachi S-4800 microscope. TEM images were collected on an FEI-Tecnai G2 20. XRD was carried out on a Shimadzu LabX XRD-6000. Raman spectroscopy was obtained using a Renishaw Micro-Raman system 2000 with He-Ne laser excitation (wavelength 623.8 nm). XPS was performed with a VG ESCALAB 250 spectrometer using a nonmonochromatized Al Kα X-ray source (1486.6 eV). The C 1s and N 1s spectra were obtained after charge correction using the binding energy of Ti 2p as reference. ICP-AES was conducted on Optima 2000 DV spectrometer. Auger electron spectroscopy with argon sputtering was obtained from PHI-700Xi equipped with a field emission source and a coaxial cylindrical mirror analyzer (5 KV, $\leq 3.9 \times 10^{-9}$ Torr). The sputtering rate was about 50 nm min^{-1}. Conductivity was measured by a four-point probe meter (RTS-8).

Electrochemical Experiments. The electrochemical measurements were carried out on PARSTAT 2273 electrochemical system by employing a typical three-electrode setup. NHC electrode (or commercial Pt/C, HC, graphite electrodes with the same catalyst loading) was used as working electrode, a platinum sheet and an Ag/AgCl (saturated KCl) electrode served as the counter electrode and the reference electrode, respectively. All potentials were quoted with respect to reversible hydrogen electrode (RHE), which were converted by the following equation: $E_{vs\ RHE} = E_{vs\ Ag/AgCl} + 0.059 \times pH + 0.199$ (V). Linear sweep voltammograms with scan rate of 5 mV s^{-1} and scan range of -0.40 ~ 0.05 V (vs RHE) were obtained in hydrogen purged 0.5 M H_2SO_4. Electrochemical impedance spectroscopy measurements were conducted at η = 0.199 V from 100000 Hz to 0.005 Hz with amplitude of 5 mV in a three-electrode system. The linear portions of the Tafel plots were fitted to the Tafel equation, $\eta = a + b\log j + jR$, where η (V) is the applied overpotential, a (V) is the Tafel constant, b (V dec^{-1}) is the Tafel slope, j (A cm^{-2}) is the current density (refers to the geometric surface area of the working electrode), R (Ω cm^{-2}) is the total area-specific uncompensated resistance of the system. The long-term durability test was conducted at a fixed potential in 0.5 M H_2SO_4 solution by recording the current density.

Electrocatalytic hydrogen production by NHC electrode was performed in a gas-tight double-chamber cell. During hydrogen production, the cathodic chamber was constantly flushed with nitrogen (2 mL/min) and the output gas was collected. To quantify hydrogen produced, the output gas was sampled (200 μL) every 2 min and analyzed in a gas chromatograph (Shimadzu, GC-14C) equipped with molecular sieve 5A column thermostated at 100°C and a thermal conductivity detector (TCD) thermostated at 120°C. Then chromatographic peak area of hydrogen (S_H) could be obtained. To get the calibration curve, hydrogen was flowed into the cathodic chamber (constantly flushed with nitrogen but without water electrolysis) with known flow rates and measured by the same procedure. A linear relationship between the chromatographic peak areas of hydrogen and the amounts of hydrogen was obtained (y = ax + b, y is the peak area, x is the hydrogen amount). According to the peak area of hydrogen (S_H) and the equation y = ax + b, the amount of hydrogen produced can be calculated. The hydrogen production efficiency was calculated as follows: production efficiency = 2nF/Q, where n is the amount of hydrogen produced (mol), F is the Faraday constant, Q is the amount of charge passed through the cell (C).

1. Danilovic, N. *et al.* Enhancing the alkaline hydrogen evolution reaction activity through the bifunctionality of $Ni(OH)_2$/metal catalysts. *Angew. Chem. Int. Ed.* **51**, 12495-12498 (2012).
2. Wang, M., Chen, L. & Sun, L. C. Recent progress in electrochemical hydrogen production with earth-abundant metal complexes as catalysts. *Energy Environ. Sci.* **5**, 6763–6778 (2012).
3. Walter, M. G. *et al.* Solar water splitting cells. *Chem. Rev.* **110**, 6446–6473 (2010).
4. Esposito, D. V. *et al.* Low-cost hydrogen-evolution catalysts based on monolayer platinum on tungsten monocarbide substrates. *Angew. Chem. Int. Ed.* **49**, 9859–9862 (2010).
5. Kibsgaard, J., Chen, Z. B., Reinecke, B. N. & Jaramillo, T. F. Engineering the surface structure of MoS_2 to preferentially expose active edge sites for electrocatalysis. *Nat. Mater.* **11**, 963–969 (2012).
6. Cobo, S. *et al.* A janus cobalt-based catalytic material for electro-splitting of water. *Nat. Mater.* **11**, 802–807 (2012).

7. Du, P. W. & Eisenberg, R. Catalysts made of earth-abundant elements (Co, Ni, Fe) for water splitting: recent progress and future challenges. *Energy Environ. Sci.* **5**, 6012–6021 (2012).
8. Thoi, V. S., Sun, Y. J., Long, J. R. & Chang, C. J. Complexes of earth-abundant metals for catalytic electrochemical hydrogen generation under aqueous conditions. *Chem. Soc. Rev.* **42**, 2388–2400 (2013).
9. Popczun, E. J. *et al.* Nanostructured nickel phosphide as an electrocatalyst for the hydrogen evolution reaction. *J. Am. Chem. Soc.* **135**, 9267–9270 (2013).
10. Anxolabehere-Mallart, E. *et al.* Boron-capped tris (glyoximato) cobalt clathrochelate as a precursor for the electrodeposition of nanoparticles catalyzing H_2 evolution in water. *J. Am. Chem. Soc.* **134**, 6104–6107 (2012).
11. Vrubel, H., Merki, D. & Hu, X. L. Hydrogen evolution catalyzed by MoS_3 and MoS_2 particles. *Energy Environ. Sci.* **5**, 6136–6144 (2012).
12. Chen, W. F. *et al.* Biomass-derived electrocatalytic composites for hydrogen evolution. *Energy Environ. Sci.* **6**, 1818–1826 (2013).
13. Liao, L. *et al.* A nanoporous molybdenum carbide nanowire as an electrocatalyst for hydrogen evolution reaction. *Energy Environ. Sci.* **7**, 387–392 (2014).
14. Chang, Y. H. *et al.* Highly efficient electrocatalytic hydrogen production by MoS(x) grown on graphene-protected 3D Ni foams. *Adv. Mater.* **25**, 756–760 (2013).
15. Li, Y. G. *et al.* MoS_2 nanoparticles grown on graphene: an advanced catalyst for the hydrogen evolution reaction. *J. Am. Chem. Soc.* **133**, 7296–7299 (2011).
16. Chen, W. F. *et al.* Highly active and durable nanostructured molybdenum carbide electrocatalysts for hydrogen production. *Energy Environ. Sci.* **6**, 943–951 (2013).
17. Wang, T. Y. *et al.* Enhanced electrocatalytic activity for hydrogen evolution reaction from self-assembled monodispersed molybdenum sulfide nanoparticles on an Au electrode. *Energy Environ. Sci.* **6**, 625–633 (2013).
18. Tran, P. D. *et al.* Copper molybdenum sulfide: a new efficient electrocatalyst for hydrogen production from water. *Energy Environ. Sci.* **5**, 8912–8916 (2012).
19. Shalom, M. *et al.* Controlled carbon nitride growth on surfaces for hydrogen evolution electrodes. *Angew. Chem. Int. Ed.* **53**, 3654–3658 (2014).
20. Zhuo, J. *et al.* Salts of $C_{60}(OH)_8$ electrodeposited onto a glassy carbon electrode: surprising catalytic performance in the hydrogen evolution reaction. *Angew. Chem. Int. Ed.* **52**, 10867–10870 (2013).
21. Panizza, M. & Cerisola, G. Application of diamond electrodes to electrochemical processes. *Electrochim. Acta* **51**, 191–199 (2005).
22. Yu, H. B., Wang, H., Quan, X., Chen, S. & Zhang, Y. B. Amperometric determination of chemical oxygen demand using boron-doped diamond (BDD) sensor. *Electrochem. Commun.* **9**, 2280–2285 (2007).
23. He, H. L., Sekine, T. & Kobayashi, T. Direct transformation of cubic diamond to hexagonal diamond. *Appl. Phys. Lett.* **81**, 610–612 (2002).
24. Liu, J. J., Watanabe, H., Fuji, M. & Takahashi, M. Electrocatalytic evolution of hydrogen on porous alumina/gelcast-derived nano-carbon network composite electrode. *Electrochem. Commun.* **11**, 107–110 (2009).
25. Stuart, E. J. E. & Pumera, M. Nanographite impurities within carbon nanotubes are responsible for their stable and sensitive response toward electrochemical oxidation of phenols. *J. Phys. Chem. C.* **115**, 5530–5534 (2011).
26. Su, D. S., Perathoner, S. & Centi, G. Nanocarbons for the development of advanced catalysts. *Chem. Rev.* **113**, 5782–5816 (2013).
27. Yokoya, T. *et al.* Origin of the metallic properties of heavily boron-doped superconducting diamond. *Nature* **438**, 647–650 (2005).
28. Zeng, A. P. *et al.* Correlation between film structures and potential limits for hydrogen and oxygen evolutions at a-C:N film electrochemical electrodes. *Carbon* **46**, 663–670 (2008).
29. Chen, X. M., Chen, G. H., Gao, F. R. & Yue, P. L. High-performance Ti/BDD electrodes for pollutant oxidation. *Environ. Sci. Technol.* **37**, 5021–5026 (2003).
30. Raole, P. M., Mukherjee, S. & John, P. I. X-ray photoelectron spectroscopic study of plasma source nitrogen ion implantation in single crystal natural diamond. *Diamond Relat. Mater.* **14**, 482–485 (2005).
31. Shalini, J. *et al.* In situ detection of dopamine using nitrogen incorporated diamond nanowire electrode. *Nanoscale* **5**, 1159–1167 (2013).
32. Vrubel, H. & Hu, X. L. Molybdenum boride and carbide catalyze hydrogen evolution in both acidic and basic solutions. *Angew. Chem. Int. Ed.* **51**, 12703–12706 (2012).
33. Laursen, A. B., Vesborg, P. C. K. & Chorkendorff, I. A high-porosity carbon molybdenum sulphide composite with enhanced electrochemical hydrogen evolution and stability. *Chem. Commun.* **49**, 4965–4967 (2013).
34. Zhen, Y. *et al.* Toward design of synergistically active carbon-based catalysts for electrocatalytic hydrogen evolution. *J. Am. Chem. Soc.* **8**, 5290–5296 (2014).

Acknowledgments

This work was supported by National Basic Research Program of China (2011CB936002) and National Nature Science Foundation of China (No.21077018).

Author contributions

Y.M.L. and X.Q. designed the experiments, Y.M.L. performed the experiments, Y.M.L., H.T.Y., S.C., H.M.Z. and Y.B.Z. analysed the data, Y.M.L. and X.Q. co-wrote the manuscript.

Additional information

Supplementary information accompanies this paper at http://www.nature.com/scientificreports

Competing financial interests: The authors declare no competing financial interests.

How to cite this article: Liu, Y. *et al.* Efficient and durable hydrogen evolution electrocatalyst based on nonmetallic nitrogen doped hexagonal carbon. *Sci. Rep.* **4**, 6843; DOI:10.1038/srep06843 (2014).